PAPER

A method of manufacturing microfluidic contact lenses by using irreversible bonding and thermoforming

View the article online for updates and enhancements.

Related content

IOP ebooks™

Bringing you innovative digital publishing with leading voices to create your essential collection of books in STEM research.

Start exploring the collection - download the first chapter of every title for free.

A method of manufacturing microfluidic contact lenses by using irreversible bonding and thermoforming

Hongbin An[1]**, Liangzhou Chen**[1] ⬤**, Xiaojun Liu**[1]**, Bin Zhao**[1]**, Donglin Ma**[2] **and Zhigang Wu**[1,3]

[1] State Key Laboratory of Digital Manufacturing Equipment and Technology, Huazhong University of Science and Technology, Wuhan 430074, People's Republic of China
[2] School of Optical and Electronic Information, Huazhong University of Science and Technology, Wuhan 430074, People's Republic of China
[3] Department of Engineering Sciences, the Angstrom Laboratory, Uppsala University, Uppsala 75121, Sweden

E-mail: chenlz@hust.edu.cn

CrossMark

Abstract

In this paper, we present the development of microfluidic contact lenses, which is based on the advantages of wearable microfluidics and can have great potential in the ophthalmology healthcare field. The development consists of two parts; the manufacturing process and the usability tests of the devices. In the manufacturing process, we firstly extended silane coupling and surface modification to irreversibly bond plastic membranes with microchannel-molded silicone rubber, to form the plastic-PDMS plane assemblies, and then molded the plane into a contact lens by thermoforming. We systematically investigated the effects of thermoforming factors, heating temperatures and the terrace die's sphere radius on channels by using the factorial experiment design. In addition, various tests were conducted to verify the usability of the devices. Through blockage and leakage tests, the devices were proved to be feasible, with no channel-blockages and could stand high pressures. Through a wearing test, the contact lenses were confirmed to be harmless on the living body. Furthermore, by performing the manipulating test, the device was proved to be liquid-controllable. These works provide a foundation for the applications of microfluidic contact lenses in ophthalmology.

Keywords: microfluidic contact lenses, thermoforming, factorial experiment, contact lens

S Supplementary material for this article is available online

(Some figures may appear in colour only in the online journal)

1. Introduction

Wearable microfluidics, incorporating microfluidics in wearable technologies, have shown great potential in healthcare applications [1], including biochemical sensing of bodily fluids (e.g. analyzing the metabolites in the sweat of glucose [2–4], lactate [2, 3] and pH [3–5]), biophysical sensing (e.g. tactile sensing [6–10], strain sensor [4, 11], bending monitoring [9, 11] and pulse pressure sensing [7]), microfluidic drug patches [12], and soft actuators [13]. By utilizing current micro-fabrication techniques and the soft, flexible, stretchable materials, those microfluidic devices are fabricated to be wearable and contain microstructures (usually microchannels) that can accurately store, hand and dispense liquids [1, 14], which provide the basis for the realization of various healthcare applications. These wearable microfluidic devices have many advantages, based on the material properties of liquids. For example, by using the conductivity of liquid metal, the micro-patterned structures can conduct with electrodes on the substrate or MEMS with superior flexibility [1, 15].

1361-6439/18/105008+10$33.00

1

Meanwhile, some devices for continuous healthcare monitoring applications can be more sensitive [6, 7], and easily monitored by smart phones [2, 3].

However, despite all the research and their advantages, the current wearable microfluidic devices all have a flexible plane enabling them to be to worn and tested on the finger, wrist, forehead or shoulder [2–13], which essentially means that the devices have only been worn with contact with our body's most common organ—the skin. In fact, our body contains many fragile and sensitive organs, like our eyes. Similarly, smart contact lenses as minimally invasive wearable platforms for ophthalmological diagnostics and treatments have emerged in recent years [16], including biochemical sensing of the tears (tears glucose monitoring [17]), biophysical sensing for intraocular pressure (IOP) [18, 19] and drug delivery contact lenses [20] (e.g. IOP lowering [21], treating Fungal keratitis [22]). Smart contact lenses have the same functions and applications as wearable microfluidics. Since wearable microfluidics have so many advantages, it is promising to incorporate microfluidics into contact lenses to develop curved microfluidic devices for ophthalmological applications.

It is hard to manufacture spherical microfluidic devices that can match the 3D curved surface of the cornea, as the micro-fabrication process for microfluidic devices is a planar process. An attempt has previously been made, John Yan tried to develop a microfluidic contact lens to monitor IOP. He made it by thermoforming a bonded full-PDMS (polydimethylsiloxane) microfluidic chip into a spherical shape against two rigid molds, immediately after it was heated to 300 °C for 5 min [23]. However, because PDMS is a thermosetting polymer [24], it cannot be softened (once cured) by heating [25], therefore its manufacturing process is theoretically difficult to achieve. Besides that, the high temperature (over 200 °C) will lead to the thermal decomposition of PDMS [26], this causes the contact lenses they prepared to age yellow and become unwearable for eyes.

To develop microfluidic contact lenses, as we know, conventional thermoplastics, widely used in the packaging industry, such as PET (polyethylene terephthalate) and PMMA (poly (methyl methacrylate)), can be thermoformed to form a variety of complex surfaces [27]. These thermoplastics have also been used as cover-plates or substrates in wearable microfluidics, so, why not use plastic–plastic or plastic–PDMS assemblies to make microfluidic contact lenses? PDMS and plastic PET have already been used in smart contact lenses and have come into contact with the cornea [18, 28]. Since PDMS is biocompatible, soft and highly oxygen-permeable, and it can be easily modified as a hydrophilic [1, 18], it is more suitable for contact with the cornea than PET. PDMS can meet the requirements of contact lenses, which include being soft, breathable and moist. The soft property makes the contact lens comfortable to wear, the others ensure the contact lens does not affect the normal physiological activities and environments of the eye [29]. So, it would be wise to use PET–PDMS assemblies and thermoform them from the PDMS side. The current wearable microfluidics, with a plastic-rubber structure, all integrate channels on the soft side [1, 9, 10]. This is mainly because the soft property can associate more

potential applications, and it would be wise for us to do the same. Moreover, in order to make PDMS not separate from the curved PET after thermoforming, the bonding strength between them needs to be strong enough. The bonding methods, surface modifications [30] and chemical coupling treatment [31] in previous research, can meet these requirement.

Here, by using PET films (cover plates) and PDMS films containing channels (substrates), we develop microfluidic contact lenses. We firstly integrated the PET–PDMS microfluidic assemblies. Then, the plane assemblies were molded to the contact lenses against the spherical drawing dies. The channels were changed after thermoforming, and so, we performed factorial experiments to investigate the effect of different thermoforming factors on the channels. Also, various tests were performed to judge and evaluate the usability of the microfluidic contact lenses.

2. Experiments

2.1. Materials

The PET films (thickness 0.2 mm) were purchased from Sumitomo Chemical (Japan). The PDMS prepolymer (Sylgard 184) and its curing agent were provided by Dow Corning (Midland, MI, USA). 3-aminopropyltriethoxysilane (APTES, 99%) was from Sigma-Aldrich (Milwaukee, WI, USA). Photoresist, SU-8 2015, SU-8 2075 and its developer were purchased from MicroChem (Newton, MA, USA). Acetone, alcohol and isopropyl alcohol (IPA) were obtained from Sinopharm Chemical Reagent (Shanghai, China).

2.2. Microchannel fabrication

A series of rectangular microchannels were fabricated in PDMS by using conventional photolithography and replica molding techniques, as shown in figure 1(a). First, SU-8 2015 or SU-8 2075 were separately spin-coated on a plasma-treated Si wafer at a corresponding rotational speed, followed by soft baking. After UV exposure under the different line-width masks by using a mask aligner (ABM/6/350/NUV/DCCD/M, ABM, Inc., USA), hard baking was performed, and next developed in SU-8 developer. Used as the mold, the prepared SU-8 master patterns were measured through an ultra-depth 3D microscope (DSX510, Olympus Inc., Japan) to confirm its actual sizes. After the patterns were rinsed clean in IPA, dried and sprayed with an atomizing mold-release agent (GA-7500, Daikin Industries, Japan), the non-curing PDMS (two components mix in a 10:1 ratio and degassed) was poured onto the mold and spin-coated at 500 rpm for 10s. After the mixing was thermally cured at 80 °C for 60 min, the PDMS replica-mold films were peeled off from the master with a thickness of approximately 600 μm.

2.3. Bonding experiments

The process of bonding the PET cover plate with the PDMS substrate is shown schematically in figure 1. A group of commercial PET films (posted up on the wafer) were used as
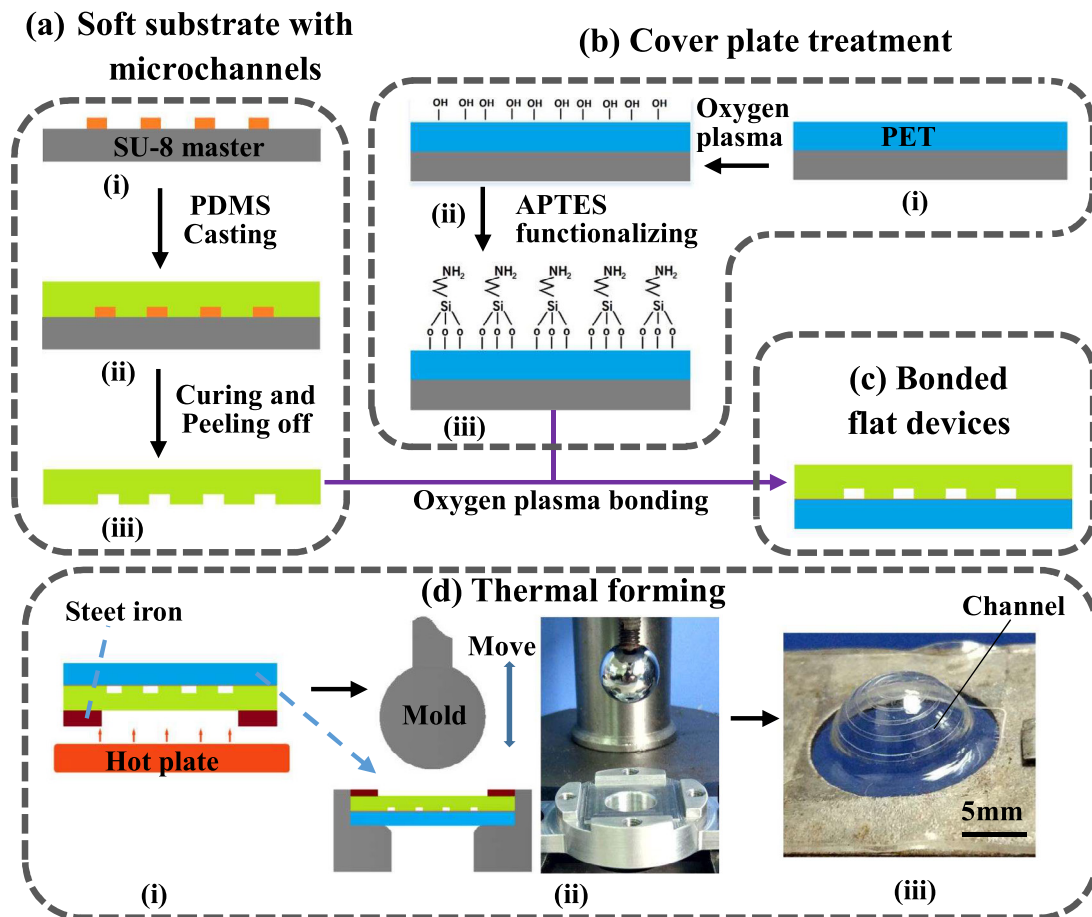
Figure 1. Schematic illustration of the fabrication of microfluidic contact lenses. (a) The schematic of process flow for manufacturing soft silicone substrate, including: (i) the microchannel SU-8 master, (ii) casting PDMS, (iii) curing and peeling off the PDMS. (b) The schematic of the process flow for PET cover plate treatment, including: (i) oxygen plasma treating, (ii) APTES-functionalizing. (c) The picture of bonded PET-PDMS assembly. (d) The schematic illustration of thermoforming progress to press the plate into the spherical cap, including: (i) heating to soften the assembly, (ii) hemispherical drawing forming, (iii) the thermoformed spherical device.

cover plates and a series of PDMS films containing different micro-channels (as described in section 2.2) were used as the substrate. In order to bond PDMS and PET with enough strength, the commercially available silane, APTES, was firstly diluted in water with 5% per volume to form a hydrolytic solution, and then used to form silylation of the surface of the PET [30], figure 1(b). More specifically, the PET membranes were firstly activated in an oxygen plasma chamber (Harrick Plasma Cleaner PDC-001, Ithaca, NY, USA) for 1 min (600 mTorr, 100 W), resulting in the hydrophilization of the PET surface. Then the members were dipped into the prepared solution for 20 min to graft a silylated layer on the surface of the PET, in which the solution was wrapped in a glass dish and heated at 80 °C on a hot plate. After that, the membranes were removed from the APTES solution, and dried in a class-1000 clean room. The PDMS substrate and the functionalized PET were next activated in an oxygen plasma chamber (600 mTorr, 100 W) for 30 s to form Si–OH groups on both surfaces. After that, the two members were immediately brought into contact, and left in an oven heated at 70 °C for 10 min. Finally, an irreversible bond was formed, as shown in figure 1(c).

2.4. Thermal forming

As shown in figure 1(d), the bonded flat plastic–silicone microfluidic assemblies were thermoformed into contact lenses. The PET–PDMS assembly was removed from the wafer and fixed to a square clip by using double-sided adhesive. The fixed device was firstly heated on the hot-plate to transform the PET from the hard 'glassy' state to the soft 'rubbery' state. After that, the device was immediately put on the concave die and then the mirrored spherical terrace die was pushed down. The heated assembly followed to stretch against the terrace die until touching the whole die. Keeping the contact of the mold for 1 min to cool the assembly down, the spherical microfluidic was finally prepared and had the same curvature as the terrace die.

2.5. Design of experiment

As the thermoforming process included 3D stretching, the positional and dimensional parameters of the rectangular channels would vary accordingly. Microchannels are the key structure to manipulate liquid precisely in microfluidics [14], so it is
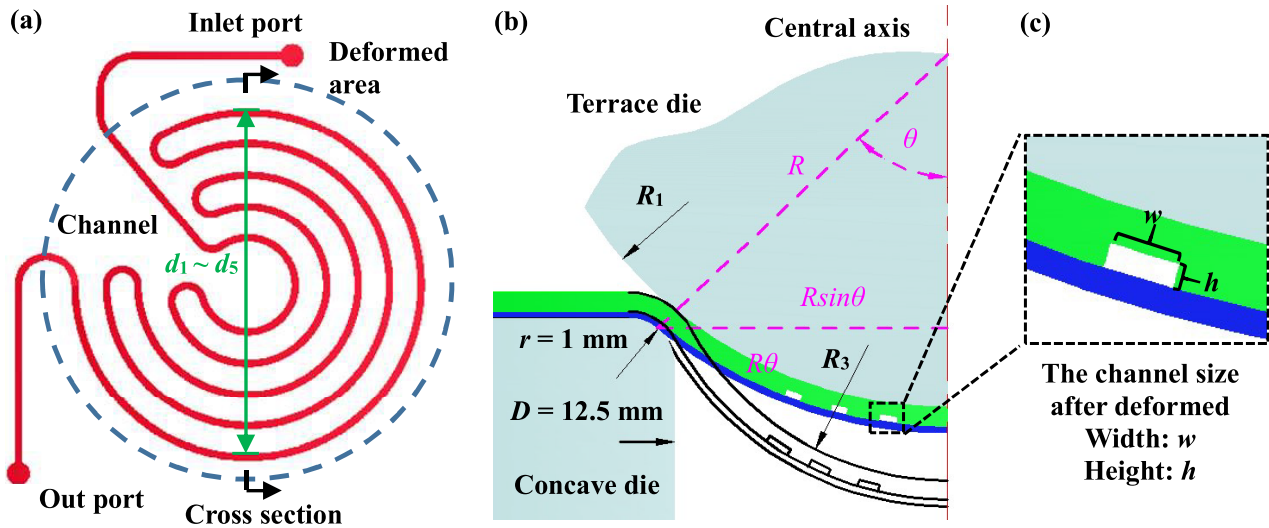
Figure 2. (a) The channel pattern; (b) the schematic diagram of the 3D stretching process; (c) the deformed channel.

Table 1. Thermoforming parameters and their variation levels.

Factors	Levels		
A: heating temperatures (°C)	A_1: 35 s at 160 °C	A_2: 35 s at 170 °C	A_3: 35 s at 180 °C
B: sphere radius of the terrace die (mm)	B_1: $R_1 = 8$ mm	B_2: $R_2 = 7$ mm	B_3: $R_3 = 6$ mm

important to explore how the thermoforming process affects the channels. The thermoforming process consisted of two steps, heating to soften and stretch forming, so the conformal experiments explorde the impact of the two corresponding factors on the channels. The PET–PDMS assembly, containing five annularly distributed channels (measuring 250.2 μm × 97.4 μm) with different diameters (d_1–d_5 = 3–11 mm), as shown in figure 2(a), was used as the experimental object (three samples in each group).

As shown in table 1, the heating temperatures were the first factor, with three levels. It controlled the softening degree of the thermoplastics. With the increase in heating temperature, the tensile strength of the PET plastic would decline. Based on the needs of contact lenses for different crowds, the sphere radius of the terrace die with three variations of 8, 7 and 6 mm was another factor. This related to the macroscopically extensibility of the deformed areas, and could be introduced by the following equations, combining figure 2(b).

$$\begin{cases} \delta = \dfrac{2R\theta - 2R\sin\theta}{2R\sin\theta} & (1) \\ D = 2R\sin\theta & (2) \end{cases}$$

where δ is the macroscopically extensibility of the deformed areas, θ is the subtended angle, R is the sphere radius, and D is the inner diameter of the hole die. With the decrease of the sphere radius, the extensibility can be calculated to increase.

2.6. Evaluating the effect of the thermoforming process on the micro-channels

The positions of the annularly distributed channels, were explored by measuring their thermoformed diameters using the Vernier caliper. The dimension parameters were measured and explored by means of scanning electron microscopy. A Helios NanoLab G3-CX instrument was utilized to observe the cross-section of the assemblies, which were sliced up in the middle and fixed on the platform. Variations of the diameter, the width (parameter: w, figure 2(c)) and height (parameter: h), under different parameters were statistically analyzed and evaluated.

2.7. Blockage and leakage tests

It was particularly important to conduct blockage and leakage tests to verify the usability of the channels. The tests were performed by introducing visible red ink into the channels, and a syringe pump (SPlab02, SHENCHEN, China) was used to provide the driving force. A syringe needle (BD-30G) was inserted into the silicon rubber injection port, to connect the channels with the silicone conduit, which had been linked with the syringe. In addition, the interfaces of every junction were glued by using a strong adhesive to prevent disengagement. For the serpentine channel with the smallest size (measuring 50 μm × 40 μm), the flow rate was maintained at 0.2 mL min^{-1} to observe whether the channel became blocked. For the large channels (measuring 250.2 μm × 97.4 μm), the flow rates were controlled at high levels of 3 and 5 ml min^{-1} to evaluate the bonding quality.

The bonding strength of the spherical devices was further measured by performing burst pressure tests [29]. A T-shaped fluidic interconnect was introduced into the front loop to connect separately with the conduit and channels, while the remaining interface was linked to a digital pressure sensor (PX273–300DI, Omega Engineering Inc., USA) for loop pressure measurement. The outlet of the channel was blocked

by using a strong adhesive, and, thus the loop pressure would increase when the loop air was compressed by the liquid injection. The red ink was controlled at a flow rate of 1 ml min^{-1} to compress the air until the burst happened.

3. Results and discussion

3.1. Effect of thermoforming on the channels

3.1.1. Effect of thermoforming on the channel positions. The annularly distributed microchannels were still distributed in a ring-shape after being thermoformed from planar to spherical. Figure 3 shows the statistical results of the measured diameters' rate of change, it can be seen that all the groups' rate of change varied from 0% to 4.5% (less than 5%). Based on the measured data, it was concluded that the temperatures and the sphere radius had no significant influence on the channels' distributions ($p > 0.05$, using the two factor ANOVA method; table S1, ESI). The result indicates that the spherical stamping process is similar to the process of mapping the annularly distributed channel from a plane to a spherical shape along the central axis.

3.1.2. Effect of the different process parameters on the channel size.

3.1.2.1.The channels' distributions and the different sphere radii effect on the channel dimensions. The sphere radius of the mold showed a remarkable influence on the channel sizes, especially on the sizes of the distributed channels on the outside ($p < 0.05$, using the two factor ANOVA method; table S1, ESI). Figure 4(a) shows the cross section of three channels with one thermoformed device (lever: A1, B2), the channels' shape after thermoforming can be observed to be trapezoidal, with an increase in width and a decrease in height. Also, the outer channels were more deformed than the inner, both in width and height; this is mainly because the outside area's strain is larger than the inside during the spherical stamping process.

Based on that, the thermoforming process does not affect the channel's distributions and it is the mapping process. So, for the small channel that has a distance of $d/2$ from the central axis, combining figure 4(b), its local extensibility can be analyzed according to the equations as follows,

$$\begin{cases} \varphi(d;R) \approx \dfrac{\frac{\Delta x}{\cos\theta} - \Delta x}{\Delta x} & (3) \\ \theta = \arcsin(\dfrac{d/2}{R + t}) & (4) \end{cases}$$

where $\varphi(d; R)$ represents the extensibility of the local small channel area, Δx is the former length of the small micro-element containing channels, $\Delta x/\cos(\theta)$ represents the thermoformed length of the small micro-element, d is the diameter of the annularly distributed channel and so $d/2$ represents the distance from the channel to the central axis, R is the sphere radius of the terrace die and contains three levels in our experiments (B$_1$–B$_3$) and t represents the thickness of the PDMS, 0.6 mm.
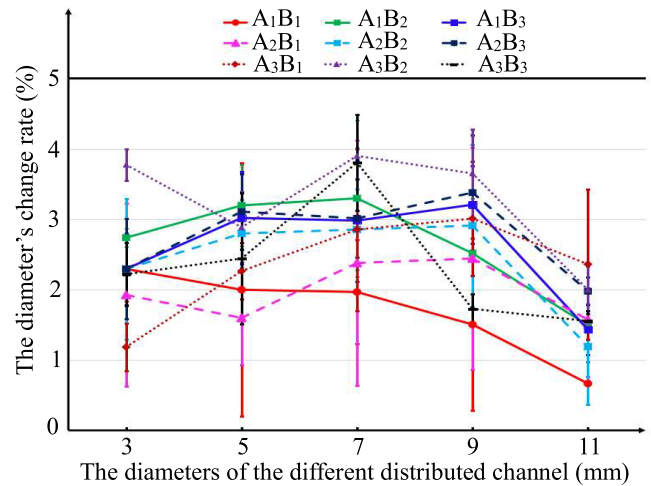
Figure 3. The diameter's rate of change of the different distributed channels after the thermoforming.

Figure 5(a) shows the width's rate of change under simulation and measurements. For channels at the same distance from the center, the larger the terrace die's sphere radius, the smaller the rate of change. Whether due to the effect of the distributions or the sphere radius, the change in trend of the measured with the simulated were consistent, but still had deviations (less than 0.15). This might have been caused by many factors such as the inconsistency of the PDMS's thickness, the measurement errors, or the small deviation in the centering of the assemblies with the mold during stamping. Figure 5(b) shows the rate of change of the measured height. The change in the trend of height was symmetrically opposite to that of the width, but smaller, and basically unchanged for the channels distributed at diameters of 3–5 mm. Figure 5(c) shows the rate of change of the channel's sectional area. With an increase in the distributed diameter or a decrease in the sphere radius, the rate of change increased; because the width's growth was faster than the decrease in height. For other groups under different temperatures, the regular patterns were the same (figures S1–S3, ESI (stacks.iop.org/JMM/28/105008/mmedia)).

3.1.2.2.The effect of heating temperature on the channel dimensions. Based on the variance analysis that a significant level of all groups was calculated to be greater than 0.05 (table S1, ESI), the heating temperatures were concluded to not play a significant impact on the channel size. Figures 6(a) and (b) show the measured width and height of the circular channel which was 7 mm in diameter at different levers. For the experimental groups in the same mold (factors B1–B3), it can be seen that the mean of the width and height changed a little under different temperature levels (factors A1–A3). The cause of the result may be the fact that in the same mold (the macroscopic elongation is the same), the different levers of the filmy PET softening was difficult at playing a significant role. Its Young's modulus at the softening stage (in soft 'rubbery' state, MPa level), was the same order of magnitude as that of the thicker PDMS. Besides that, we also tried to increase the heating temperatures to conduct more experiments to explore
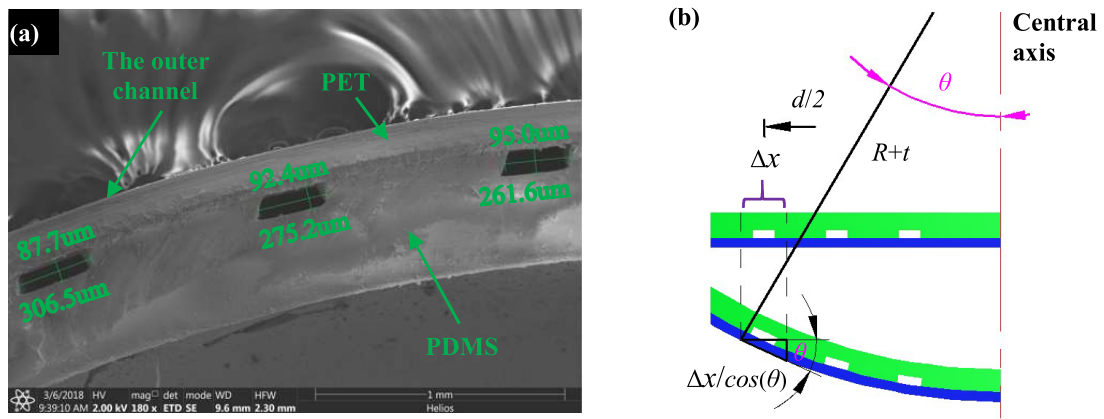
Figure 4. (a) The cross section of channels (lever: A1, B2); (b) the picture for analyzing the extensibility of the local small channel area.
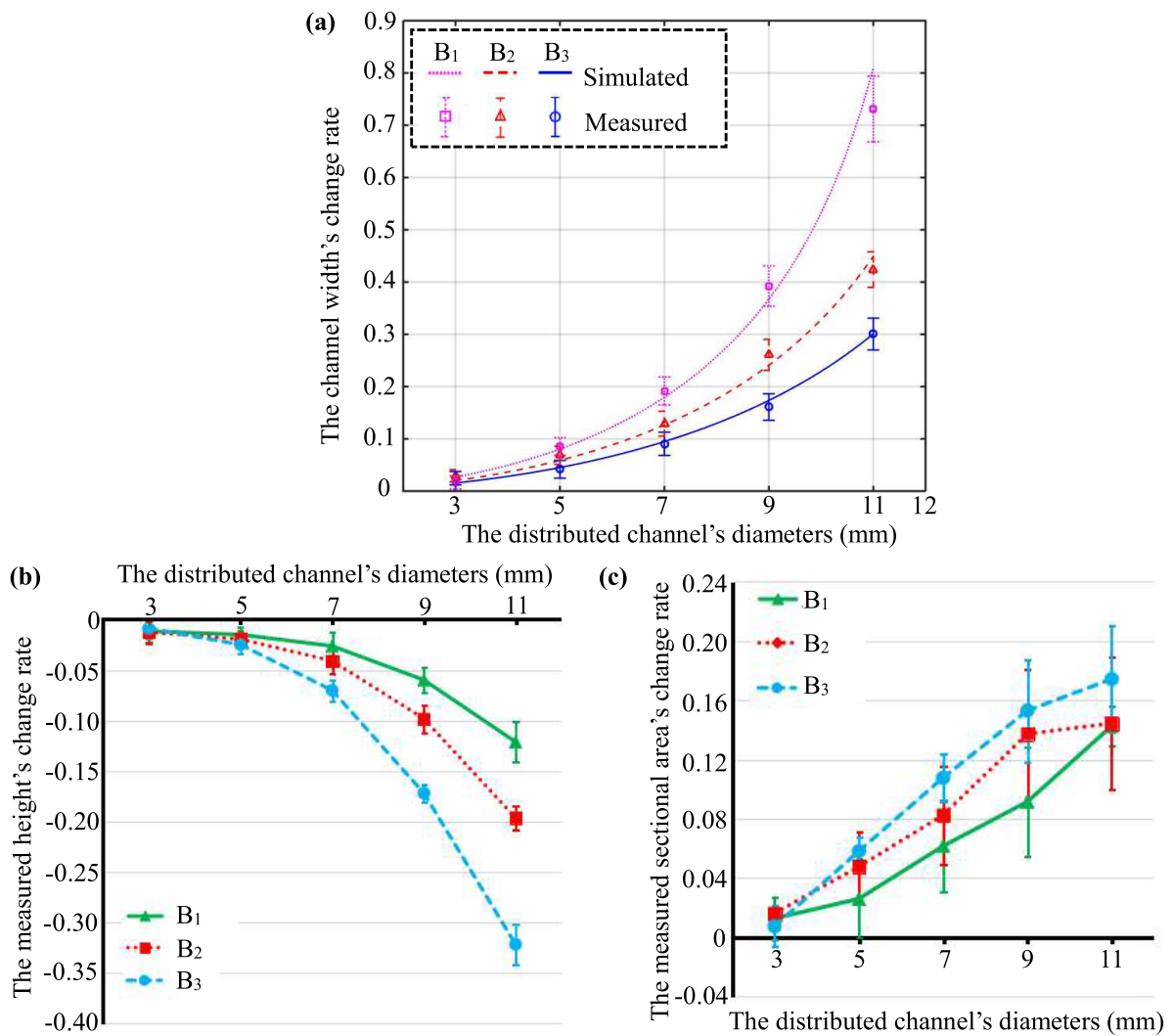
Figure 5. (a) The simulated and measured rate of change (width) of the different distributed channels under the action of different terrace dies with the same heating temperatures (A_2); (b) the rate of change of the measured height; (b) the rate of change of the measured channel's sectional area.
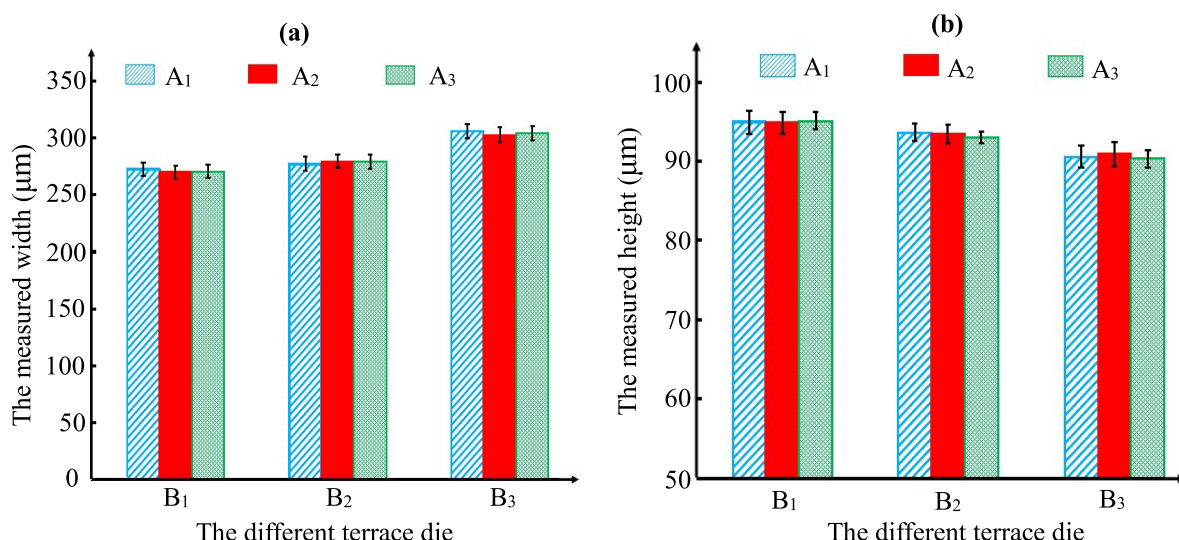
Figure 6. The measured width and height of the circular channel with a diameter of 7 mm under the action of different temperature levels, and (a) the width, (b) the height; no significant difference was observed between every group with the same mold based on the ANOVA ($p > 0.05$).
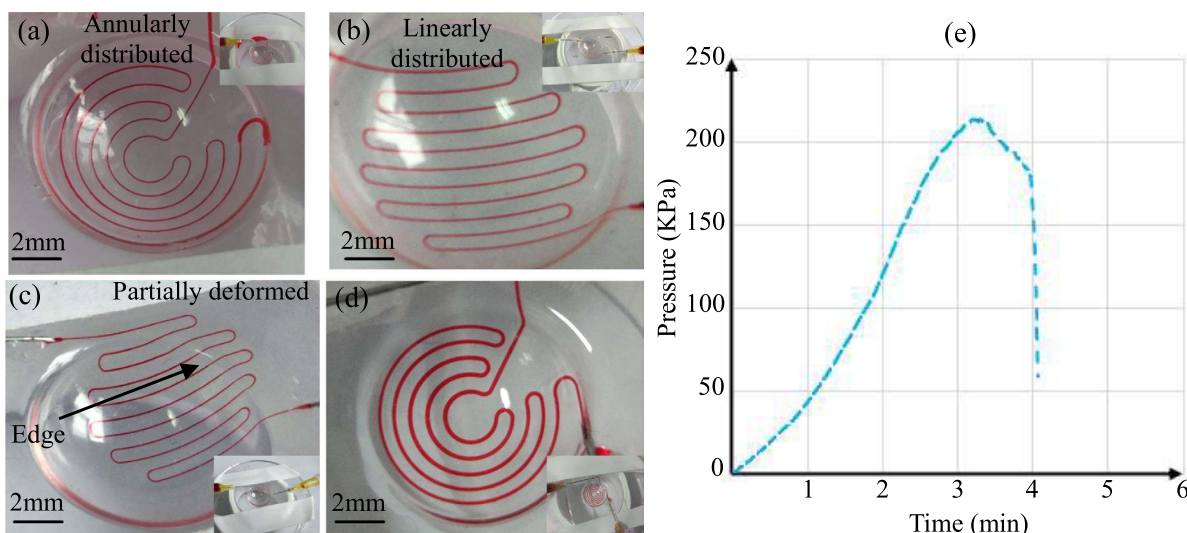
Figure 7. Results of blockage and leakage tests. (a)–(c) Introduction of red solution passed through the smallest channel without blocking and (a) the channels annularly distributed, (b) the channels linearly distributed, (c) with partial channels deformed and cross the large deformed edge; (d) introduction of the channel tolerated the strong influx of the liquid without delamination at the highest flow rate of 5 ml min^{-1}; (e) burst pressure test.

the impact, but the films were bleached during heating at temperatures of 190 °C.

3.2. Blockage and leakage tests

Figure 7 shows the results of the liquid injection tests, which were carried out to examine the usability of the channels. The test results (see section 1 in the movie of ESI) indicate that no blockages were caused by thermoforming, the red ink could easily pass through channels as small as 50 μm × 40 μm; even with the channel linearly distributed or partly deformed and crossing the large deformed edge, as shown in figures 7(a)–(c). Moreover, for each high flow rate of the large channel, the red solution could pass through it without separation or leakage. The channel was still in good condition even at the highest flow

rate of 5 ml min^{-1}, as shown in figure 7(d). In view of the total internal volume of the channel (measured 3.61 μl), the assembly withstood a violent inburst of the fluid whose injected volume per-minute was nearly 1400-times greater than the channel. This verifies that the connection strength was sufficient.

Figure 7(e) shows the whole process of the pressure change during the burst test, and the strength was good enough. When the pressure rose to the extent that the liquid was injected to compress the air, the connection of the pressure sensor with the T-shaped interconnect was broken from the device. The bonding strength of the thermoformed PET–PDMS assembly was measured at over 213 KPa (30.9 Psi), it satisfies that needed for microfluidic devices [32]. As a result, our above tests confirm that the devices were feasible, with no channel-blockages and could stand high pressures.
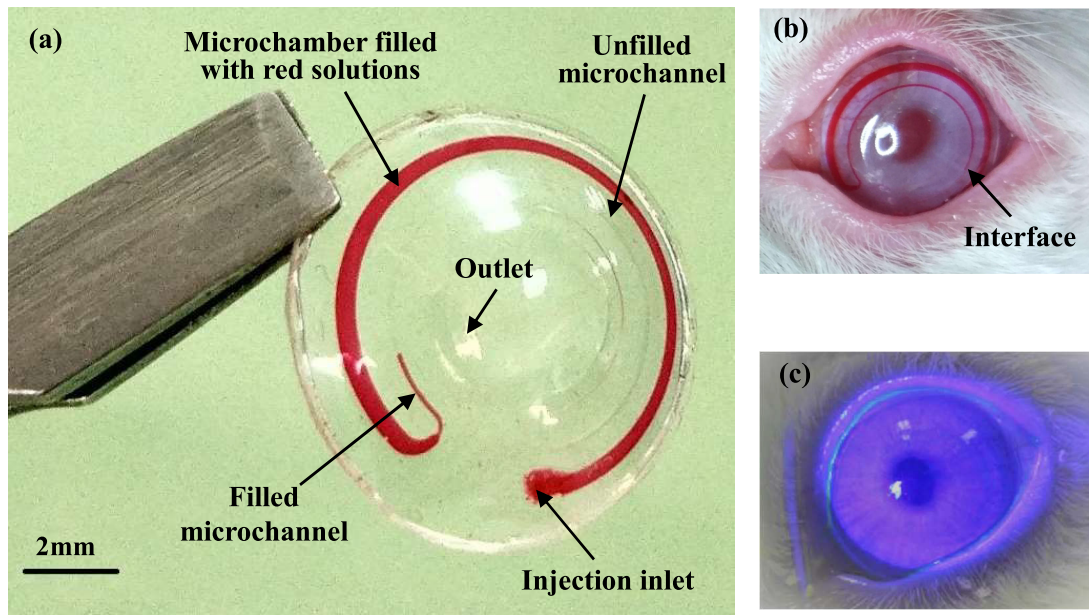
Figure 8. (a) Diagram of the wearable microfluidic contact lenses including filled microchanmber, microchannel filled with liquid in some regions, injection inlet and outlet; (b) the contact lens being worn on the rabbit's eye; (c) the cornea fluorescence test shows that the contact lens caused no corneal injury.
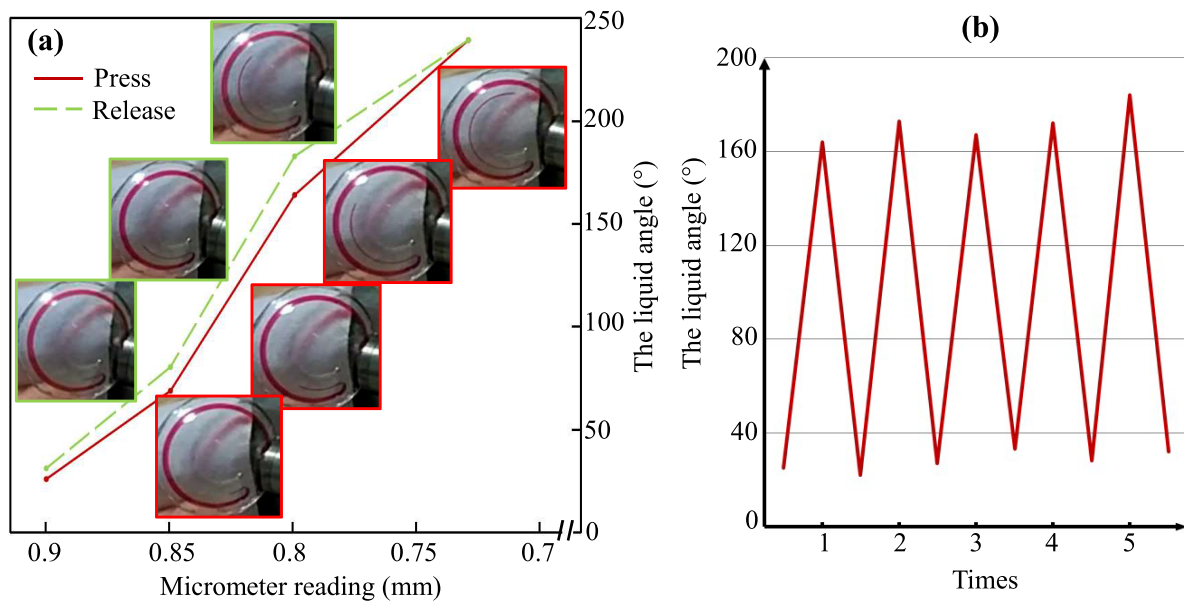
Figure 9. Results of manipulating test. (a) Measurement of relative change of the liquid angle in the small channel at different deformation distances from 0.9–0.73 mm under the reciprocating action of a micrometer; (b) dynamic test of the inlet region circularly pressed between 0.9–0.8 mm.

3.3. Wearing and manipulating tests of wearable microfluidic contact lenses

According to the manufacturing process, a microfluidic contact lens (curvature radius: 8.0 mm, and containing channels of 101.1 μm × 58.8 μm and 502 μm × 146.1 μm) was made with its outer edge cut off. A controlled volume of red glycerol solution (2.26 μl) was infused into the channel network and then the injection inlet was sealed up. The large channel (microchamber) and the entrance point of the smaller channel were filled with the red liquid, as shown in figure 8(a).

The wearing test was conducted with the point of view that contact lenses should be harmless to sensitive and fragile eyes.

Before the test, the device was treated by corona discharge (BD-10ASV, Electro-Technic Products) for 1 min to modify the PDMS surface to become hydrophilic. Then the device was put on the eye of the anaesthetized experimental rabbit. Figure 8(b) shows that the device fitted the rabbit's cornea well. When the contact lens had just been worn on the eyes, the interface of the red liquid moved forward, this was mainly caused by the extrusion of the eyelids. Then, with time, the interface of the red liquid was found to change slowly and ceaselessly, this might have been caused by the small movement of the eyelids or the corneal deformation (caused by the IOP fluctuation). After 8 h of being worn, the contact lens was

taken away and a drop of fluorescein was applied on the rabbit's cornea. Then, the cornea was observed under cobalt blue light. As shown in figure 8(c), no fluorescence discoloration (turn green) was found on the corneal surface. The result indicates that the device caused no corneal abrasion, since such damage would lead to corneal surface roughness, resulting in the accumulation of fluorescein and then the green discoloration. As a result, the test indicates that wearing these contact lenses was harmless.

Since liquid manipulability is the basic property of microfluidic devices [14], for wearable microfluidic contact lenses, a simple experiment was conducted to verify its performance by means of a micrometer. Figure 9(a) shows the result (see section 2 in the movie of ESI) that the fluid flowed forward and the liquid angle (the angle between the end of the red liquid and the entrance point of the small channel) increased when the injection inlet region was pressed by the micrometric screw, with the reading changing from 0.9–0.73 mm. In turn, as the micrometric screw reversed, the fluid flowed back due to the vacuum force generated from the PDMS recovery. Figure 9(b) shows the round-trip test of the inlet region circularly pressed and released between 0.9–0.8 mm, indicating good repeatability (the deviation was less than 20°). The test indicates that the microfluidic contact lens was liquid-controllable.

Based on liquid manipulability, microfluidic contact lenses will be studied for much ophthalmology healthcare research and many applications. For example, the 'micrometer pressure' can be replaced by IOP, by using the optical detector to measure the displacement of the red liquid in real-time, the device will be used to measure and monitor IOP continuously. Also, the red liquid can be replaced by liquid drugs (like eyedrops), and then the microfluidic contact lens may be studied for automatic and real-time drug delivery to treat ophthalmological diseases.

Conclusion

We developed microfluidic contact lenses, based on their promising applications in the ophthalmology healthcare field. The process consisteded of two parts, the manufacturing process and usability tests. In the manufacturing process, by using PET members and PDMS films containing channels, we bonded them irreversibly to form the plane plastic–PDMS assemblies first and then thermoformed them to the contact lenses. The effect of the different thermoforming parameters on the channels was studied by using the factorial experiment. We have shown that the process does not remarkably affect the channel distributions, and the spherical stamping process was similar to the process of mapping the annular distributed channel from plane to spherical along the central axis. The die's sphere radius and the channel distributions showed a significant influence on the channel size; where the width and height's rate of change of the same distributed channel increased with a decrease in the radius. Moreover, the sizes of the outer distributed channels changed more than the inner channels in the same group. The heating temperatures showed no evident influence on the channel sizes.

Usability tests of the microfluidic contact lenses were also conducted. Through blockage and leakage tests, the inside channels of the devices were proved to be usable, the process could integrate a microchannel with a minimum size of 50 μm × 40 μm to the spherical. Through the wearing test, the contact lenses, when worn, were proved to be harmless to the living body. While the manipulating test was conducted and verified that the devices were liquid-controllable. Based on these characteristics, the microfluidic contact lenses are good prospects for studying various healthcare applications in ophthalmology.

ORCID iDs

Liangzhou Chen ⬤ https://orcid.org/0000-0002-5403-691X

References

[1] Yeo J C and Lim C T 2016 Emergence of microfluidic wearable technologies *Lab Chip* **16** 4082–90
[2] Gao W *et al* 2016 Fully integrated wearable sensor arrays for multiplexed *in situ* perspiration analysis *Nature* **529** 509–14
[3] Koh A, Kang D, Xue Y, Lee S, Pielak R M, Kim J and Manco M C 2016 A soft, wearable microfluidic device for the capture, storage, and colorimetric sensing of sweat *Sci. Transl. Med.* **8** 366ra165
[4] Mostafalu P *et al* 2016 A toolkit of thread-based microfluidics, sensors, and electronics for 3D tissue embedding for medical diagnostics *Microsyst. Nanoeng.* **2** 16039
[5] Curto V F *et al* 2012 Real-time sweat pH monitoring based on a wearable chemical barcode micro-fluidic platform incorporating ionic liquids *Sensors Actuators* B **171** 1327–34
[6] Nie B, Li R, Brandt J D and Pan T 2014 Microfluidic tactile sensors for three-dimensional contact force measurements *Lab Chip* **14** 4344–53
[7] Nie B, Li R, Brandt J D and Pan T 2014 Iontronic microdroplet array for flexible ultrasensitive tactile sensing *Lab Chip* **14** 1107–16
[8] Yeo J C, Yu J, Koh Z M, Wang Z and Lim C T 2016 Wearable tactile sensor based on flexible microfluidics *Lab Chip* **16** 3244–50
[9] Yeo J C, Yu J, Shang M, Loh K P and Lim C T 2016 Highly flexible graphene oxide nanosuspension liquid-based microfluidic tactile sensor *Small* **12** 1593–604
[10] Yeo J C, Yu J, Loh K P, Wang Z and Lim C T 2016 Triple-state liquid-based microfluidic tactile sensor with high flexibility, durability, and sensitivity *ACS Sensors* **1** 543–51
[11] Jeong S H, Zhang S, Hjort K, Hilborn J and Wu Z 2016 PDMS-based elastomer tuned soft, stretchable, and sticky for epidermal electronics *Adv. Mater.* **28** 5830–6
[12] Wang H *et al* 2016 Triboelectric liquid volume sensor for self-powered lab-on-chip applications *Nano Energy* **23** 80–8

[13] Polygerinos P *et al* 2015 Soft robotic glove for combined assistance and at-home rehabilitation *Robot. Auton. Syst.* **73** 135–43

[14] Whitesides G M 2006 The origins and the future of microfluidics *Nature* **442** 368

[15] Cheng S and Wu Z 2012 Microfluidic electronics *Lab Chip* **12** 2782–91

[16] Farandos N M, Yetisen A K, Monteiro M J, Lowe C R and Yun S H 2015 Contact lens sensors in ocular diagnostics *Adv. Healthcare Mater.* **4** 792–810

[17] Yao H *et al* 2012 A contact lens with integrated telecommunication circuit and sensors for wireless and continuous tear glucose monitoring *J. Micromech. Microeng.* **22** 075007

[18] Leonardi M *et al* 2009 Wireless contact lens sensor for intraocular pressure monitoring: assessment on enucleated pig eyes *Acta Ophthalmol.* **87** 433–7

[19] Chen G Z *et al* 2013 Capacitive contact lens sensor for continuous non-invasive intraocular pressure monitoring *Sensors Actuators* A **203** 112–8

[20] Xinming L *et al* 2008 Polymeric hydrogels for novel contact lens-based ophthalmic drug delivery systems: a review *Contact Lens Anterior Eye* **31** 57–64

[21] Peng C C *et al* 2012 Extended drug delivery by contact lenses for glaucoma therapy *J. Control. Release* **162** 152–8

[22] Huang J F *et al* 2016 A hydrogel-based hybrid theranostic contact lens for fungal keratitis *ACS Nano* **10** 6464–73

[23] Yan J 2011 An unpowered, wireless contact lens pressure sensor for point-of-care glaucoma diagnosis *33rd Annual Int. Conf. on Engineering in Medicine and Biology Society of the IEEE EMBS* pp 2522–5

[24] Armani D K and Liu C 2000 Microfabrication technology for polycaprolactone, a biodegradable polymer *J. Micromech. Microeng.* **10** 80

[25] Blaga A 1978 Use of plastics in solar energy applications *Solar Energy* **21** 331–8

[26] Liu M, Sun J and Chen Q 2009 Influences of heating temperature on mechanical properties of polydimethylsiloxane *Sensors Actuators* A **151** 42–5

[27] Wu Z, Jobs M, Rydberg A and Hjort K 2015 Hemispherical coil electrically small antenna made by stretchable conductors printing and plastic thermoforming *J. Micromech. Microeng.* **25** 027004

[28] Lingley A R *et al* 2011 A single-pixel wireless contact lens display *J. Micromech. Microeng.* **21** 125014

[29] Quintero V *et al* 2017 Stretchable electronic platform for soft and smart contact lens applications *Adv. Mater. Technol.* **2** 1700073

[30] Eddings M A, Johnson M A and Gale B K 2008 Determining the optimal PDMS–PDMS bonding technique for microfluidic devices *J. Micromech. Microeng.* **18** 067001

[31] Vlachopoulou M E *et al* 2009 A low temperature surface modification assisted method for bonding plastic substrates *J. Micromech. Microeng.* **19** 15007

[32] Sia S K and Whitesides G M 2003 Microfluidic devices fabricated in poly (dimethylsiloxane) for biological studies *Electrophoresis* **24** 3563–76